

Pressure-Induced Superconductivity and Structural Phase Transitions in Magnetic Topological Insulator Candidate MnSb_4Te_7

Cuiying Pei^{1#}, Ming Xi^{2#}, Qi Wang^{1,3}, Wujun Shi^{4,5}, Lingling Gao¹, Yi Zhao¹, Shangjie Tian², Weizheng Cao¹, Changhua Li¹, Mingxin Zhang¹, Shihao Zhu¹, Yulin Chen^{1,3,6}, Hechang Lei^{2*}, and Yanpeng Qi^{1,3,7*}

1. School of Physical Science and Technology, ShanghaiTech University, Shanghai 201210, China
2. Department of Physics and Beijing Key Laboratory of Opto-electronic Functional Materials & Micro-nano Devices, Renmin University of China, Beijing 100872, China
3. ShanghaiTech Laboratory for Topological Physics, ShanghaiTech University, Shanghai 201210, China
4. Center for Transformative Science, ShanghaiTech University, Shanghai 201210, China
5. Shanghai High Repetition Rate XFEL and Extreme Light Facility (SHINE), ShanghaiTech University, Shanghai 201210, China
6. Department of Physics, Clarendon Laboratory, University of Oxford, Parks Road, Oxford OX1 3PU, UK
7. Shanghai Key Laboratory of High-resolution Electron Microscopy, ShanghaiTech University, Shanghai 201210, China

These authors contributed to this work equally.

* Correspondence should be addressed to Y.P.Q. (qiyp@shanghaitech.edu.cn) or H.C.L. (hlel@ruc.edu.cn)

ABSTRACT:

The magnetic van der Waals crystals $(\text{MnX}_2\text{Te}_4)_m(\text{X}_2\text{Te}_3)_n$ ($\text{X} = \text{Sb}, \text{Bi}$) have drawn significant attention due to their rich topological properties and the tenability by external magnetic field. In this work, we report on the discovery of superconductivity in magnetic topological insulator candidate MnSb_4Te_7 ($m = 1, n = 1$) via the application of high pressure. The antiferromagnetic ordering is robust to pressure until 8 GPa and then fully suppressed. The carrier type converts from hole- to electron-type accompanied with structural phase transition at around 15 GPa. Superconductivity emerges near the critical pressure 30 GPa where MnSb_4Te_7 converted into a simple cubic phase. Interestingly, MnSb_4Te_7 shows a dome-like phase diagram with a maximum T_c of 2.2 K at 50.7 GPa. The results

demonstrate that MnSb_4Te_7 with nontrivial topology of electronic states display new ground states upon compression.

INTRODUCTION

Superconductivity and topological quantum state are two important fields of frontier research in condensed matter physics. Since the discovery of topological insulators (TIs), extensive investigations have been conducted for observing topological superconductivity (TSC) and Majorana fermions, which have potential applications to fault-tolerant topological quantum computation.¹⁻⁴ One feasible route to realize topological superconductor is to search for intrinsic superconductivity in topological materials by doping/intercalation or applying high pressure.⁵⁻¹⁸ Indeed, superconductivity achieved in this manner has been observed in typical topological insulators. For example, topological insulator Bi_2Se_3 can be induced to become a bulk superconductor, by copper intercalation in the van der Waals gaps between the Bi_2Se_3 layers or application of pressure above 11 GPa.^{5, 19}

When magnetic ordering is introduced to topological insulators, such intrinsic magnetic topological insulators (MTIs) can display a lot of unusual physical properties, such as Chern insulator state with chiral edge state hosting quantum anomalous Hall effect and axion insulator state with axion electrodynamics²⁰⁻²³. Recently, intrinsic MTIs of $(\text{MnBi}_2\text{Te}_4)_m(\text{Bi}_2\text{Te}_3)_n$ has been theoretically predicted and experimentally synthesized to have tunable magnetic properties and topologically nontrivial surface states²²⁻³⁶. $(\text{MnBi}_2\text{Te}_4)_m(\text{Bi}_2\text{Te}_3)_n$ crystallizes in a typical van der Waals layered structure, sharing a similar crystal structure with Bi_2Te_3 , a typical TI under ambient conditions. Although the topological properties of these materials have been intensively studied in the past few years, no superconductivity has been observed either by chemical doping or apply pressure.

Compared with $(\text{MnBi}_2\text{Te}_4)_m(\text{Bi}_2\text{Te}_3)_n$, the $(\text{MnSb}_2\text{Te}_4)_m(\text{Sb}_2\text{Te}_3)_n$ family remains much less explored. In particular, MnSb_4Te_7 ($m = 1$, $n = 1$), one member of the $(\text{MnSb}_2\text{Te}_4)_m(\text{Sb}_2\text{Te}_3)_n$ family, is a magnetic topological system with versatile topological phases that can be manipulated by both carrier doping and magnetic field³⁷.

In this work, we report on the discovery of superconductivity on intrinsic MTI candidate MnSb_4Te_7 via the application of high pressure. Application of pressure effectively tunes physical properties and crystal structure of MnSb_4Te_7 . Pressure-induced two high-pressure phase transitions are revealed in MnSb_4Te_7 , and superconductivity with a dome shape behavior is observed after MnSb_4Te_7 converts into a simple cubic phase.

EXPERIMENTAL SECTION

Sample preparation. Sample synthesis, structural and composition characterizations. Single crystals of MnSb_4Te_7 were grown using the self-flux method. The starting materials Mn (piece, 99.99%), Sb (grain, 99.9999%), and Te (lump, 99.9999%) were mixed in an Ar-filled glove box at a molar ratio of Mn : Sb : Te = 1 : 11.5 : 15. The mixture was placed in an alumina crucible, which was then sealed in an evacuated quartz tube. The tube was heated to 1023 K for 24 h and kept at that temperature for 20 h. Then, the tube was slowly cooled down to 881 K at a rate of 0.5 K/h followed by separating the crystals from the flux by centrifuging. Finally, the ampoule was taken out from the furnace and decanted with a centrifuge to separate MnSb_4Te_7 single crystals from the flux. MnSb_4Te_7 single crystals are stable in the air. The phase and quality examinations of MnSb_4Te_7 single crystal were performed on the Bruker AXS D8 Advance powder crystal x-ray diffractometer with Cu $K_{\alpha 1}$ ($\lambda = 1.54178 \text{ \AA}$) at room temperature. Magnetotransport measurements were performed on Physical Property Measurement System (PPMS). The magnetization measurement was carried on a Magnetic Property Measurement System (MPMS).

High pressure measurements. High pressures were generated with diamond anvil cell (DAC) as described elsewhere³⁸⁻⁴¹. *In situ* high-pressure x-ray diffraction (XRD) measurements were performed at beamline BL15U of Shanghai Synchrotron Radiation Facility (x-ray wavelength $\lambda = 0.6199 \text{ \AA}$). A symmetric DAC with 200 μm culet was used with rhenium gasket. Silicon oil was used as the pressure transmitting medium (PTM) and pressure was determined by the ruby luminescence method⁴². The two-dimensional diffraction images were analyzed using the FIT2D software⁴³. Rietveld refinements on crystal structures under high pressure were performed using the General

Structure Analysis System (GSAS) and the graphical user interface EXPGUI⁴⁴⁻⁴⁵. An *in situ* high-pressure Raman spectroscopy investigation on MnSb₄Te₇ was performed by a Raman spectrometer (Renishaw in-Via, UK) with a laser excitation wavelength of 532 nm and low-wavenumber filter. A symmetry DAC with 200 μm culet was used, with silicon oil as the PTM. *In situ* high-pressure resistivity and Hall effect measurements of MnSb₄Te₇ were conducted on a nonmagnetic DAC. A piece of nonmagnetic BeCu was used as the gasket. Cubic BN/epoxy mixture layer was inserted between BeCu gasket and electrical leads as insulator layer. Four Pt foils were arranged according to the van der Pauw method. To monitor the evolution of T_N , NaCl was used as PTM to get a quasi-hydrostatic pressure to the sample.

RESULTS AND DISCUSSION

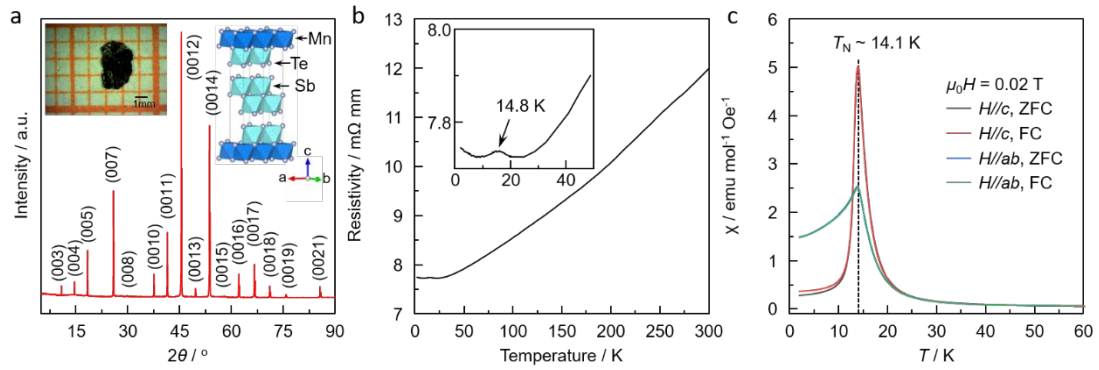


Figure 1. (a) The room temperature x-ray diffraction peaks from the ab plane of MnSb₄Te₇ crystal. Inset: Image of a typical MnSb₄Te₇ single crystal synthesized in this work and the schematic crystal structure of MnSb₄Te₇; (b) Temperature dependent of ab -plane resistivity $\rho(T)$ at zero magnetic field. Insets show the enlarged view of the $\rho(T)$ curve from 0 to 50 K; (c) The temperature dependent magnetic susceptibility χ under $\mu_0 H = 0.02$ T for $H//c$ (black and red lines) and $H//ab$ plane (blue and green lines).

At ambient pressure, MnSb₄Te₇ adopts a rhombohedral $P\bar{3}m1$ structure with alternate stacking of one MnSb₂Te₄ septuple layers (SLs) and one Sb₂Te₃ quintuple layer (QLs), as shown in the right inset of Figure 1a. All of peaks in the XRD pattern of a crystal can be well indexed by the $(00l)$ reflections of MnSb₄Te₇ (Figure 1a), indicating that the crystal surface is parallel to the ab plane and perpendicular to the c axis. A photograph of a typical MnSb₄Te₇ crystal is shown in Figure 1a, with the dimensions of about $3 \times 2 \times 0.02$ mm³. At ambient pressure, MnSb₄Te₇ crystal reveals a metallic behavior (Figure 1b). MnSb₄Te₇ exhibits an AFM transition at $T_N = 14.8$ K³⁷, and

correspondingly it leads to a kink in the resistivity $\rho(T)$ curve as shown in the inset of Figure 1b. AFM ordering temperature is further confirmed by the magnetic susceptibility presented in Figure 1c. The magnetic susceptibility decreases dramatically below T_N for $H//c$, but only slightly decreases for $H//ab$, unveiling an anisotropic AFM exchange with the c axis being the magnetic easy axis.

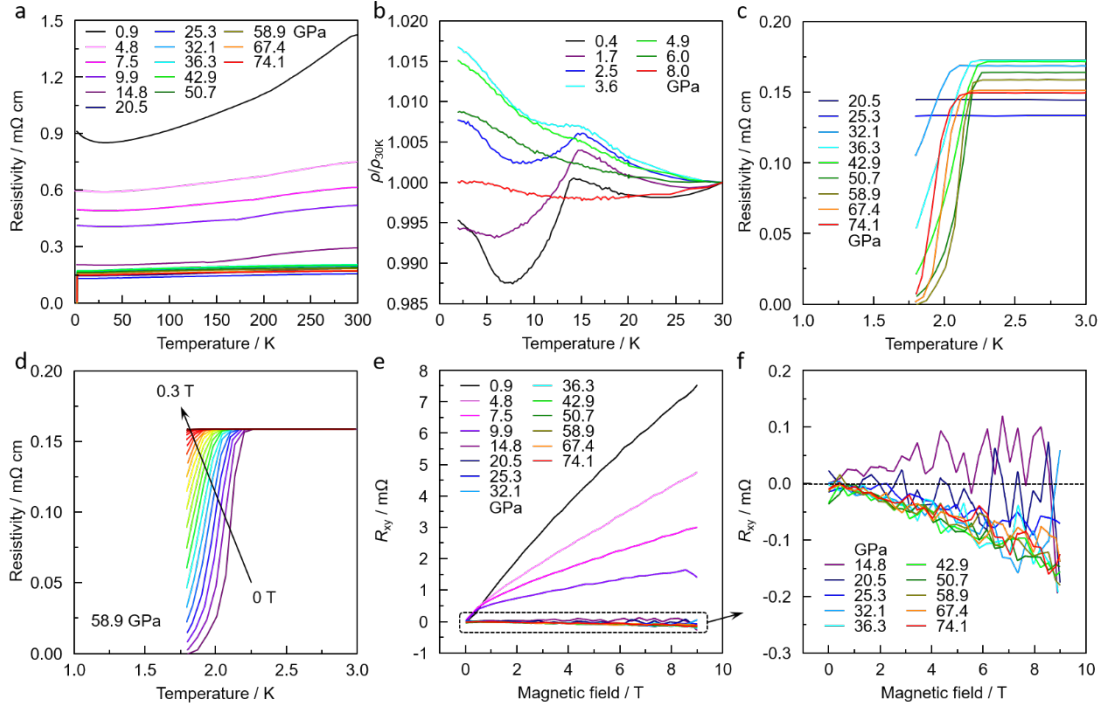


Figure 2. (a) Electrical resistivity of MnSb₄Te₇ as a function of temperature under high pressures in run III; (b) Temperature-dependent resistivity of MnSb₄Te₇ in the vicinity of the magnetic transition; (c) Temperature-dependent resistivity of MnSb₄Te₇ in the vicinity of the superconducting transition; (d) Temperature dependence of resistivity under different magnetic fields for MnSb₄Te₇ at 58.9 GPa; (e) and (f) Hall resistance of MnSb₄Te₇ as a function of magnetic field under various pressures at 10 K in run III.

Next, we measured the $\rho(T)$ of several MnSb₄Te₇ crystals under various pressures. Figure 2 shows the typical $\rho(T)$ curves of MnSb₄Te₇ up to 74.1 GPa. The sample exhibits metallic behavior in the whole pressure range. Increasing the pressure induces a continuous suppression of the overall magnitude of $\rho(T)$. It is well-known that AFM metallic ground state of MnBi₂Te₄ and MnBi₄Te₇ single crystal is gradually suppressed by pressure^{29,35}. In order to obtain the trend of the AFM ordering temperature with pressure, a 400-micron culet DAC (BeCu) was used to produce a hydrostatic environment with NaCl as PTM. Figure 2b shows the detail of the normalized low-temperature resistivity of MnSb₄Te₇ as a function of temperature at various pressures

to monitor the shift of the AFM transition kink. Unexpectedly, T_N was insensitive to pressure until 8 GPa, which is notably different from MnBi_2Te_4 and MnBi_4Te_7 ^{29,35}. Since the interlayer distance decreases under high pressure, it is speculated that the pressure-induced enhancement of AFM/FM competition and the partial delocalization of Mn-3d electrons do not destroy long-range AFM order at low pressure region.

At a pressure of 32.1 GPa, a small resistivity drop appears at 1.9 K, indicating a superconducting phase transition (Figure 2c). Upon further increasing pressure, the critical temperature of superconductivity, T_c , gradually increases with pressure, and the maximum T_c of 2.2 K is attained at $P = 50.7$ GPa, as shown in Figure 2c. Beyond this pressure, T_c decreases slowly, showing a dome-like behavior. Significantly, the T_c of MnSb_4Te_7 is lower than that of Sb_2Te_3 ¹³, which confirms the superconductivity is intrinsic and not derived from the latter. To gain further insight into the superconducting state, the temperature-dependent resistivity with an applied magnetic field was performed. As shown in Figure 2d, T_c is suppressed progressively by magnetic fields, and a magnetic field of $\mu_0 H = 0.3$ T deletes all signs of superconductivity above 1.8 K. Here, we determined T_c as the 90% drop of the normal state resistivity. The $\mu_0 H_{c2}$ versus T_c can be fitted well with Ginzburg-Landau formula: $\mu_0 H_{c2}(T) = \mu_0 H_{c2}(0)(1 - t^2)/(1 + t^2)$, where t is the reduced temperature T/T_c . The obtained $\mu_0 H_{c2}(T)$ is 0.8 T and coherence length ξ is 20.3 nm (Figure S1).

MnBi_4Te_7 and MnSb_4Te_7 are sister compounds with the same structure (inset of Figure 1a) at ambient conditions. Both MnBi_4Te_7 and MnSb_4Te_7 show metallic behavior but the carrier type is opposite (electron-type for MnBi_4Te_7 and hole-type for MnSb_4Te_7). In order to trace the evolution of charge carriers upon compression, high-pressure Hall resistivity measurements was performed on MnSb_4Te_7 with pressure up to 74.1 GPa. Figures 2e and 2f display the Hall resistance curves $R_{xy}(H)$ under various pressures. At 0.9 GPa, the Hall resistance curve exhibits a linear feature with a positive slope, indicating a hole-type conduction in agreement with the previous reports³⁷. With increasing the external pressure, the slope of the Hall resistance decreases dramatically and changes from positive to negative at 20.5 GPa, which implies a carrier-type

inversion from hole- to electron-type. The carrier concentration is extracted from Hall measurements and the jump of carrier concentration coincides with the carrier-type inversion (Figure 4 and Figure S2). Above the critical pressure, the carrier concentration increases slowly.

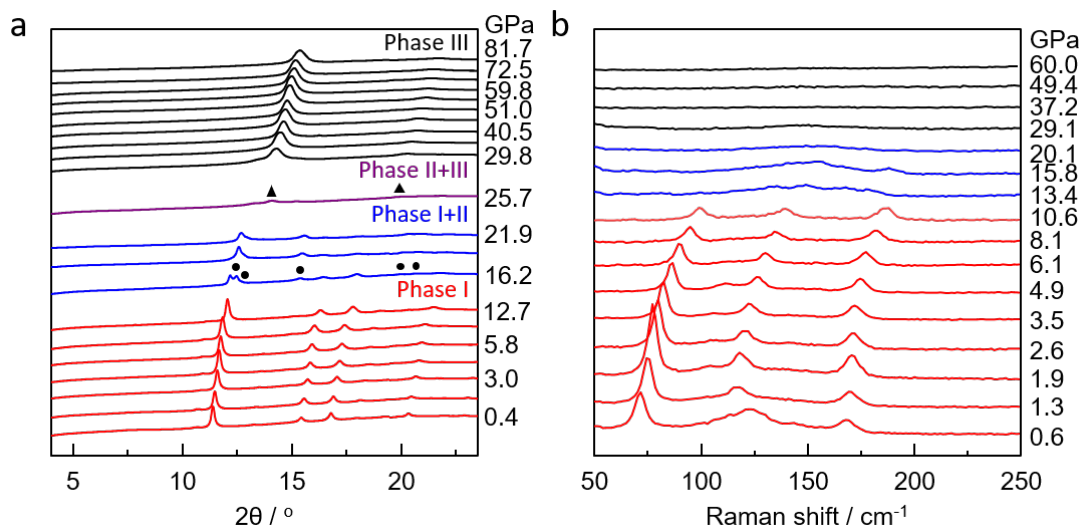


Figure 3. (a) XRD patterns of MnSb₄Te₇ measured at room temperature with increasing of external pressure up to 81.7 GPa. The x-ray diffraction wave-length λ is 0.6199 Å. Red, blue, purple and black curves are used to distinguish the structure transformation; (b) Raman spectra at various pressures for MnSb₄Te₇ at room temperature.

In order to understand the underlying mechanism of the suppressed magnetism and induced superconductivity in MnSb₄Te₇ upon compression, we did an *in situ* study on structure evolutions by using synchrotron XRD and Raman spectroscopy, as presented in Figure 3. In the low-pressure range, all the diffraction peaks of MnSb₄Te₇ could be indexed to the rhombohedral $P\bar{3}m1$ structure, indicating robust ambient structure until $P \leq 12.7$ GPa (Figure S3). At 16.2 GPa, a high-pressure phase, phase II, was observed shown in Figure 3a. This phase is only stable in a narrow pressure range upon compression. Structure searches for this system by CALYPSO method⁴⁶⁻⁴⁸ is failed since its complicated atom configuration. The Le Bail refinements for the high-pressure XRD data showed phase II attributed to monoclinic in space group $C2/m$. with $a = 14.2265(7)$ Å, $b = 3.8992(6)$ Å, $c = 16.7398(5)$ Å, and $\beta = 147.45(2)^\circ$ at 21.9 GPa. On further increasing the pressure, MnSb₄Te₇ converted into a simple cubic phase with space group $Im\bar{3}m$ at 25.7 GPa. Interestingly, we obtained a pure phase III in the pressure range of 29.8 - 81.7 GPa. After a full pressure release, MnSb₄Te₇ recovers the

ambient-pressure structure, indicating the reversible phase transition. The structural evolution of MnSb_4Te_7 under high pressure resembles the situation in the case of Sb_2Te_3 ¹³. The compression behavior is related to the distortion of MnTe_6 and SbTe_6 octahedra, which is similar to the close relative MnBi_4Te_7 ³⁵. The pressure-induced structure evolution of MnSb_4Te_7 is also confirmed by *in situ* Raman spectroscopy measurements (Figure 3b). With increasing pressure, the profile of the spectra remains similar to that at ambient pressure until 13.4 GPa, then new vibration modes appear, thus showing the first structural transition. An abrupt disappearance of Raman peaks for pressure at 29.1 GPa indicates the structural transition to phase III. The evolution of the Raman spectra is consistent with the synchrotron XRD patterns. In a word, the results of synchrotron XRD together with Raman spectroscopy provide a clear evidence of pressure-induced structural transitions in MnSb_4Te_7 .

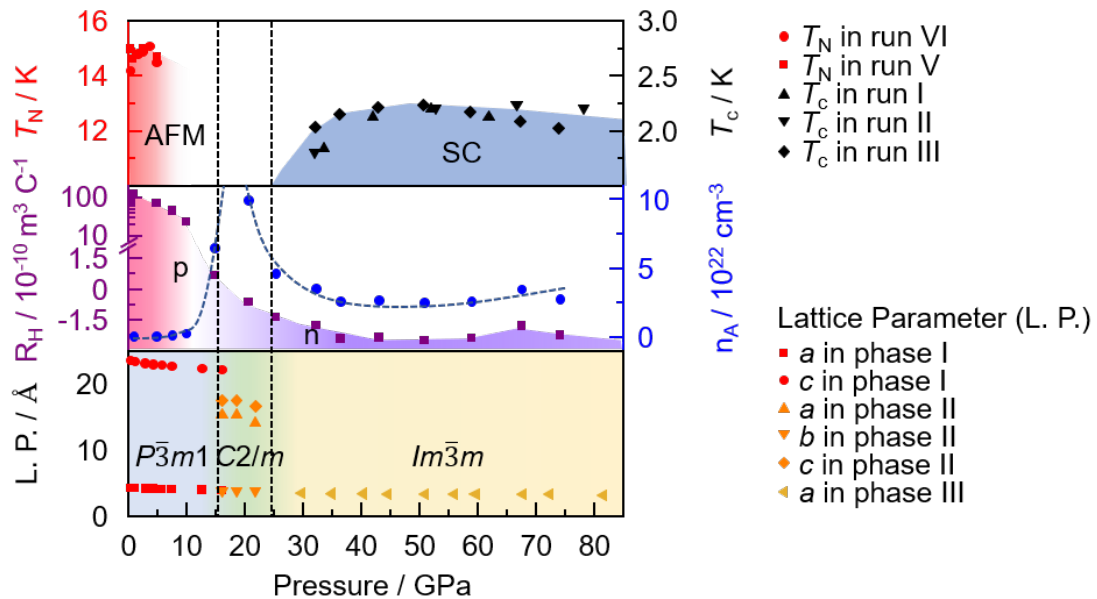


Figure 4. Phase diagram of MnSb_4Te_7 . The upper panel shows the pressure dependence of T_c and T_N . The middle panel shows the pressure dependence of Hall coefficient and carrier concentration at 10 K. The lower panel shows the lattice parameters as function of pressure.

The measurements on different samples of MnSb_4Te_7 provide the consistent and reproducible results, confirming that this superconductivity under pressure is intrinsic (Figure S4 and S5). The pressure dependences of the transition temperatures T_N/T_c , Hall resistance $R_{xy}(H)$, together with structural data obtained from the above measurements for MnSb_4Te_7 are mapped into the phase diagram shown in Figure 4. As a typical van

der Waals material, the application of pressure induced two structure transitions in MnSb_4Te_7 . For phase I ($P\bar{3}m1$), MnSb_4Te_7 show a typical AFM behavior with $T_N \sim 14.8$ K. Interestingly, AFM ordering is robust at low pressure region, which is notably different from MnBi_2Te_4 and MnBi_4Te_7 ³⁵. First structural transition appears at around 15 GPa accompanying with the elimination of AFM ordering. At the same time, the conduction changes from hole- to electron-type carrier, probable due to the reconstruction of Fermi surface. Phase II is only stable in a narrow pressure range and coexists with the phase I or the phase III upon compression. At around 25.7 GPa, MnSb_4Te_7 converted into a simple cubic phase, accompanying by the appearance of superconductivity. The T_c increases with applied pressure and reaches a maximum value of 2.2 K at 50.7 GPa for MnSb_4Te_7 , followed by a slow decrease, showing a dome shape phase diagram.

For MnSb_4Te_7 at ambient pressure, Mn d -orbitals have large contribution around the E_F ³⁷. Although atom coordination of Mn in phase III remains elusive, this large contribution of Mn d -orbital to density of states should not change significantly. The strong magnetism of Mn is commonly believed to be antagonistic to superconductivity. For a long time, manganese (Mn) is the only $3d$ element that does not show superconductivity among any Mn-based compounds, even though a great effort has been devoted recently to exploring the possible superconductivity via carrier doping or the application of high pressure. Recently, MnP was found to be the first Mn-based superconductor with transition temperature ~ 1 K under 8 GPa⁴⁹. Another example is pressure-induced superconductivity in MnSe, where the interfacial effect between the metallic and insulating boundaries may play an important role⁵⁰. Here in MnSb_4Te_7 system, superconductivity is observed accompanying with the structural transitions and suppression of AFM ordering, our results highlight that the possible antiferromagnetic spin fluctuations and pressure-induced cubic structure may be important for the appearance of superconductivity in MnSb_4Te_7 . The mechanisms of pressure-induced structural and superconducting transitions in MnSb_4Te_7 deserve further studies.

In summary, we have performed a comprehensive high-pressure study on the electrical

transport properties and crystal structures of the intrinsic MTIs MnSb_4Te_7 . Application of pressure effectively tunes crystal structure of MnSb_4Te_7 . Superconductivity with a dome shape behavior is observed for the first time after MnSb_4Te_7 converts into a simple cubic phase. Considering both intriguing magnetic topology and superconductivity in this material, our results call for further experimental and theoretical studies on MnSb_4Te_7 and related materials for a better understanding of the relation between magnetic and superconductivity, and its potential application in realizing topological superconductivity.

ACKNOWLEDGMENT

We thank Prof. Hanyu Liu for valuable discussions. This work was supported by the National Natural Science Foundation of China (Grant No. 12004252, U1932217, 11974246), the National Key R&D Program of China (Grant No. 2018YFA0704300 and 2018YFE0202600), the Natural Science Foundation of Shanghai (Grant No. 19ZR1477300), the Science and Technology Commission of Shanghai Municipality (Grant No. 19JC1413900), Shanghai Science and Technology Plan (Grant No. 21DZ2260400) and the Beijing Natural Science Foundation (Grant No. Z200005). The authors thank the support from Analytical Instrumentation Center (# SPST-AIC10112914), SPST, ShanghaiTech University. The authors thank the staffs from BL15U1 at Shanghai Synchrotron Radiation Facility for assistance during data collection.

REFERENCES

1. Hasan, M. Z.; Kane, C. L., Colloquium: topological insulators. *Rev. Mod. Phys.* **2010**, *82* (4), 3045-3067.
2. Qi, X.-L.; Zhang, S.-C., Topological insulators and superconductors. *Rev. Mod. Phys.* **2011**, *83* (4), 1057-1110.
3. Qi, X.-L.; Zhang, S.-C., The quantum spin Hall effect and topological insulators. *Phys. Today* **2010**, *63* (1), 33-38.
4. Moore, J. E., The birth of topological insulators. *Nature* **2010**, *464* (7286), 194-198.
5. Hor, Y. S.; Williams, A. J.; Checkelsky, J. G.; Roushan, P.; Seo, J.; Xu, Q.; Zandbergen, H. W.; Yazdani, A.; Ong, N. P.; Cava, R. J., Superconductivity in $\text{Cu}_x\text{Bi}_2\text{Se}_3$ and its implications for pairing in the undoped topological insulator. *Phys. Rev. Lett.* **2010**, *104* (5), 057001.
6. Liu, Z.; Yao, X.; Shao, J.; Zuo, M.; Pi, L.; Tan, S.; Zhang, C.; Zhang, Y., Superconductivity with Topological Surface State in $\text{Sr}_x\text{Bi}_2\text{Se}_3$. *J. Am. Chem. Soc.* **2015**, *137* (33), 10512-10515.

7. Qiu, Y.; Sanders, K. N.; Dai, J.; Medvedeva, J. E.; Wu, W.; Ghaemi, P.; Vojta, T.; Hor, Y. S., Time reversal symmetry breaking superconductivity in topological materials **2015**, arXiv:1512.03519.
8. Kriener, M.; Segawa, K.; Ren, Z.; Sasaki, S.; Ando, Y., Bulk superconducting phase with a full energy gap in the doped topological insulator $\text{Cu}_x\text{Bi}_2\text{Se}_3$. *Phys. Rev. Lett.* **2011**, *106* (12), 127004.
9. Andersen, L.; Wang, Z.; Lorenz, T.; Ando, Y., Nematic superconductivity in $\text{Cu}_{1.5}(\text{PbSe})_5(\text{Bi}_2\text{Se}_3)_6$. *Phys. Rev. B* **2018**, *98* (22), 220512.
10. Sasaki, S.; Segawa, K.; Ando, Y., Superconductor derived from a topological insulator heterostructure. *Phys. Rev. B* **2014**, *90* (22), 220504.
11. Zhang, J.; Zhang, S.; Weng, H.; Zhang, W.; Yang, L.; Liu, Q.; Feng, S.; Wang, X.; Yu, R.; Cao, L.; Wang, L.; Yang, W.; Liu, H.; Zhao, W.; Zhang, S.; Dai, X.; Fang, Z.; Jin, C., Pressure-induced superconductivity in topological parent compound Bi_2Te_3 . *Proc. Natl. Acad. Sci. U.S.A.* **2011**, *108* (1), 24-28.
12. Zhang, C.; Sun, L.; Chen, Z.; Zhou, X.; Wu, Q.; Yi, W.; Guo, J.; Dong, X.; Zhao, Z., Phase diagram of a pressure-induced superconducting state and its relation to the Hall coefficient of Bi_2Te_3 single crystals. *Phys. Rev. B* **2011**, *83* (14), 140504(R).
13. Zhu, J.; Zhang, J. L.; Kong, P. P.; Zhang, S. J.; Yu, X. H.; Zhu, J. L.; Liu, Q. Q.; Li, X.; Yu, R. C.; Ahuja, R.; Yang, W. G.; Shen, G. Y.; Mao, H. K.; Weng, H. M.; Dai, X.; Fang, Z.; Zhao, Y. S.; Jin, C. Q., Superconductivity in topological insulator Sb_2Te_3 induced by pressure. *Sci. Rep.* **2013**, *3*, 2016.
14. Pan, X. C.; Chen, X.; Liu, H.; Feng, Y.; Wei, Z.; Zhou, Y.; Chi, Z.; Pi, L.; Yen, F.; Song, F.; Wan, X.; Yang, Z.; Wang, B.; Wang, G.; Zhang, Y., Pressure-driven dome-shaped superconductivity and electronic structural evolution in tungsten ditelluride. *Nat. Commun.* **2015**, *6*, 7805.
15. Kang, D.; Zhou, Y.; Yi, W.; Yang, C.; Guo, J.; Shi, Y.; Zhang, S.; Wang, Z.; Zhang, C.; Jiang, S.; Li, A.; Yang, K.; Wu, Q.; Zhang, G.; Sun, L.; Zhao, Z., Superconductivity emerging from a suppressed large magnetoresistant state in tungsten ditelluride. *Nat. Commun.* **2015**, *6*, 7804.
16. Qi, Y.; Naumov, P. G.; Ali, M. N.; Rajamathi, C. R.; Schnelle, W.; Barkalov, O.; Hanfland, M.; Wu, S. C.; Shekhar, C.; Sun, Y.; Süß, V.; Schmidt, M.; Schwarz, U.; Pippel, E.; Werner, P.; Hillebrand, R.; Forster, T.; Kampert, E.; Parkin, S.; Cava, R. J.; Felser, C.; Yan, B.; Medvedev, S. A., Superconductivity in Weyl semimetal candidate MoTe_2 . *Nat. Commun.* **2016**, *7*, 11038.
17. Qi, Y.; Shi, W.; Naumov, P. G.; Kumar, N.; Schnelle, W.; Barkalov, O.; Shekhar, C.; Borrmann, H.; Felser, C.; Yan, B.; Medvedev, S. A., Pressure driven superconductivity in the transition metal pentatelluride HfTe_5 . *Phys. Rev. B* **2016**, *94*, 054517.
18. Zhou, Y.; Wu, J.; Ning, W.; Li, N.; Du, Y.; Chen, X.; Zhang, R.; Chi, Z.; Wang, X.; Zhu, X.; Lu, P.; Ji, C.; Wan, X.; Yang, Z.; Sun, J.; Yang, W.; Tian, M.; Zhang, Y.; Mao, H. K., Pressure-induced superconductivity in a three-dimensional topological material ZrTe_5 . *Proc. Natl. Acad. Sci. U S A* **2016**, *113* (11), 2904-2909.
19. Kirshenbaum, K.; Syers, P. S.; Hope, A. P.; Butch, N. P.; Jeffries, J. R.; Weir, S. T.; Hamlin, J. J.; Maple, M. B.; Vohra, Y. K.; Paglione, J., Pressure-induced unconventional superconducting phase in the topological insulator Bi_2Se_3 . *Phys. Rev. Lett.* **2013**, *111* (8), 087001.
20. Qi, X.-L.; Hughes, T. L.; Zhang, S.-C., Topological field theory of time-reversal invariant insulators. *Phys. Rev. B* **2008**, *78* (19), 195424.
21. Wang, P.; Ge, J.; Li, J.; Liu, Y.; Xu, Y.; Wang, J., Intrinsic magnetic topological insulators. *Innovation (N Y)* **2021**, *2* (2), 100098.
22. Li, J.; Li, Y.; Du, S.; Wang, Z.; Gu, B.-L.; Zhang, S.-C.; He, K.; Duan, W.; Xu, Y., Intrinsic magnetic topological insulators in van der Waals layered MnBi_2Te_4 family materials. *Sci. Adv.* **2019**, *5*,

eaaw5685.

23. Otkrov, M. M.; Klimovskikh, I.; Bentmann, H.; Estyunin, D.; Zeugner, A.; Aliev, Z. S.; Gass, S.; Wolter, A. U. B.; Koroleva, A. V.; Shikin, A. M.; Blanco-Rey, M.; Hoffmann, M.; Rusinov, I. P.; Vyazovskaya, A. Y.; Ereemeev, S. V.; Koroteev, Y. M.; Kuznetsov, V. M.; Freyse, F.; Sanchez-Barriga, J.; Amiraslanov, I. R.; Babanly, M. B.; Mamedov, N. T.; Abdullayev, N. A.; Zverev, V. N.; Alfonsov, A.; Kataev, V.; Buchner, B.; Schwier, E. F.; Kumar, S.; Kimura, A.; Petaccia, L.; Di Santo, G.; Vidal, R. C.; Schatz, S.; Kissner, K.; Unzelmann, M.; Min, C. H.; Moser, S.; Peixoto, T. R. F.; Reinert, F.; Ernst, A.; Echenique, P. M.; Isaeva, A.; Chulkov, E. V., Prediction and observation of an antiferromagnetic topological insulator. *Nature* **2019**, *576*, 416-422.
24. Wu, J.; Liu, F.; Sasase, M.; Ienaga, K.; Obata, Y.; Yukawa, R.; Horiba, K.; Kumigashira, H.; Okuma, S.; Inoshita, T.; Hosono, H., Natural van der Waals heterostructures with tunable magnetic and topological states. *Sci. Adv.* **2019**, *5*, eaax9989.
25. Gong, Y.; Guo, J.; Li, J.; Zhu, K.; Liao, M.; Liu, X.; Zhang, Q.; Gu, L.; Tang, L.; Feng, X.; Zhang, D.; Li, W.; Song, C.; Wang, L.; Yu, P.; Chen, X.; Wang, Y.; Yao, H.; Duan, W.; Xu, Y.; Zhang, S.-C.; Ma, X.; Xue, Q.-K.; He, K., Experimental realization of an intrinsic magnetic topological insulator. *Chin. Phys. Lett.* **2019**, *36*, 076801.
26. Zhang, D.; Shi, M.; Zhu, T.; Xing, D.; Zhang, H.; Wang, J., Topological axion states in the magnetic insulator MnBi_2Te_4 with the quantized magnetoelectric effect. *Phys. Rev. Lett.* **2019**, *122*, 206401.
27. Hu, C.; Gordon, K. N.; Liu, P.; Liu, J.; Zhou, X.; Hao, P.; Narayan, D.; Emmanouilidou, E.; Sun, H.; Liu, Y.; Brawer, H.; Ramirez, A. P.; Ding, L.; Cao, H.; Liu, Q.; Dessau, D.; Ni, N., A van der Waals antiferromagnetic topological insulator with weak interlayer magnetic coupling. *Nat. Commun.* **2020**, *11*, 97.
28. Chen, Y.; Xu, L.; Li, J.; Li, Y.; Wang, H.; Zhang, C.; Li, H.; Wu, Y.; Liang, A.; Chen, C.; Jung, S. W.; Cacho, C.; Mao, Y.; Liu, S.; Wang, M.; Guo, Y.; Xu, Y.; Liu, Z.; Yang, L.; Chen, Y., Topological electronic structure and its temperature evolution in antiferromagnetic topological insulator MnBi_2Te_4 . *Phys. Rev. X* **2019**, *9*(4), 041040.
29. Chen, K.; Wang, B.; Yan, J.-Q.; Parker, D. S.; Zhou, J.-S.; Uwatoko, Y.; Cheng, J.-G., Suppression of the antiferromagnetic metallic state in the pressurized MnBi_2Te_4 single crystal. *Phys. Rev. Mater.* **2019**, *3*(9), 094201.
30. Hao, Y.-J.; Liu, P.; Feng, Y.; Ma, X.-M.; Schwier, E. F.; Arita, M.; Kumar, S.; Hu, C.; Lu, R. e.; Zeng, M.; Wang, Y.; Hao, Z.; Sun, H.-Y.; Zhang, K.; Mei, J.; Ni, N.; Wu, L.; Shimada, K.; Chen, C.; Liu, Q.; Liu, C., Gapless surface Dirac cone in antiferromagnetic topological insulator MnBi_2Te_4 . *Phys. Rev. X* **2019**, *9*(4), 041038.
31. Li, H.; Gao, S.; Duan, S.; Xu, Y.; Zhu, K.; Tian, S.; Gao, J.; Fan, W.; Rao, Z.; Huang, J.; Li, J.; Yan, D.; Liu, Z.; Liu, W.; Huang, Y.; Li, Y.; Liu, Y.; Zhang, G.; Zhang, P.; Kondo, T.; Shin, S.; Lei, H.; Shi, Y.; Zhang, W.; Weng, H.; Qian, T.; Ding, H., Dirac surface states in intrinsic magnetic topological insulators EuSn_2As_2 and $\text{MnBi}_{2n}\text{Te}_{3n+1}$. *Phys. Rev. X* **2019**, *9*(4), 041039.
32. Deng, Y.; Yu, Y.; Shi, M.; Xu, Z.; Wang, J.; Chen, X.; Zhang, Y., Quantum anomalous Hall effect in intrinsic magnetic topological insulator MnBi_2Te_4 . *Science* **2020**, *367*, 895-900.
33. Zhang, S.; Wang, R.; Wang, X.; Wei, B.; Chen, B.; Wang, H.; Shi, G.; Wang, F.; Jia, B.; Ouyang, Y.; Xie, F.; Fei, F.; Zhang, M.; Wang, X.; Wu, D.; Wan, X.; Song, F.; Zhang, H.; Wang, B., Experimental observation of the gate-controlled reversal of the anomalous Hall effect in the intrinsic magnetic topological insulator MnBi_2Te_4 device. *Nano Lett.* **2020**, *20*, 709-714.
34. Liu, C.; Wang, Y.; Li, H.; Wu, Y.; Li, Y.; Li, J.; He, K.; Xu, Y.; Zhang, J.; Wang, Y., Robust axion

insulator and Chern insulator phases in a two-dimensional antiferromagnetic topological insulator. *Nat. Mater.* **2020**, *19* (5), 522-527.

35. Pei, C.; Xia, Y.; Wu, J.; Zhao, Y.; Gao, L.; Ying, T.; Gao, B.; Li, N.; Yang, W.; Zhang, D.; Gou, H.; Chen, Y.; Hosono, H.; Li, G.; Qi, Y., Pressure-Induced topological and structural phase transitions in an antiferromagnetic topological insulator. *Chin. Phys. Lett.* **2020**, *37* (6), 066401.

36. Yin, Y.; Ma, X.; Yan, D.; Yi, C.; Yue, B.; Dai, J.; Zhao, L.; Yu, X.; Shi, Y.; Wang, J.-T.; Hong, F., Pressure-driven electronic and structural phase transition in intrinsic magnetic topological insulator MnSb_2Te_4 . *Phys. Rev. B* **2021**, *104* (17), 174114.

37. Huan, S.; Zhang, S.; Jiang, Z.; Su, H.; Wang, H.; Zhang, X.; Yang, Y.; Liu, Z.; Wang, X.; Yu, N.; Zou, Z.; Shen, D.; Liu, J.; Guo, Y., Multiple magnetic topological phases in bulk van der Waals crystal MnSb_4Te_7 . *Phys. Rev. Lett.* **2021**, *126* (24), 246601.

38. Pei, C.; Jin, S.; Huang, P.; Vymazalova, A.; Gao, L.; Zhao, Y.; Cao, W.; Li, C.; Nemes-Incze, P.; Chen, Y.; Liu, H.; Li, G.; Qi, Y., Pressure-induced superconductivity and structure phase transition in Pt_2HgSe_3 . *npj Quantum Mater.* **2021**, *6*, 98.

39. Pei, C.; Shi, W.; Zhao, Y.; Gao, L.; Gao, J.; Li, Y.; Zhu, H.; Zhang, Q.; Yu, N.; Li, C.; Cao, W.; Medvedev, S. A.; Felser, C.; Yan, B.; Liu, Z.; Chen, Y.; Wang, Z.; Qi, Y., Pressure-induced a partial disorder and superconductivity in quasi-one-dimensional Weyl semimetal $(\text{NbSe}_4)_2$. *Mater. Today Phys.* **2021**, *21*, 100509.

40. Wang, Q.; Kong, P.; Shi, W.; Pei, C.; Wen, C.; Gao, L.; Zhao, Y.; Yin, Q.; Wu, Y.; Li, G.; Lei, H.; Li, J.; Chen, Y.; Yan, S.; Qi, Y., Charge Density Wave Orders and Enhanced Superconductivity under Pressure in the Kagome Metal CsV_3Sb_5 . *Adv. Mater.* **2021**, e2102813.

41. Qi, Y.; Shi, W.; Naumov, P. G.; Kumar, N.; Sankar, R.; Schnelle, W.; Shekhar, C.; Chou, F. C.; Felser, C.; Yan, B.; Medvedev, S. A., Topological quantum phase transition and superconductivity induced by pressure in the bismuth tellurohalide BiTeI . *Adv. Mater.* **2017**, *29*, 1605965.

42. Mao, H. K.; Xu, J.; Bell, P. M., Calibration of the ruby pressure gauge to 800 kbar under quasi-hydrostatic conditions. *J. Geophys. Res.* **1986**, *91* (B5), 4673-4676.

43. Hammersley, A. P.; Svensson, S. O.; Hanfland, M.; Fitch, A. N.; Hausermann, D., Two-dimensional detector software: From real detector to idealised image or two-theta scan. *High Press. Res.* **1996**, *14* (4-6), 235-248.

44. Larson, A. C.; Dreele, R. B. V., General structure analysis system (GSAS). *Los Alamos National Laboratory Report LAUR* **2004**, 86-748.

45. Toby, B., EXPGUI, a graphical user interface for GSAS. *J. Appl. Crystallogr.* **2001**, *34* (2), 210-213.

46. Wang, Y.; Lv, J.; Zhu, L.; Ma, Y., Crystal structure prediction via particle-swarm optimization. *Phys. Rev. B* **2010**, *82* (9), 094116.

47. Wang, Y.; Lv, J.; Zhu, L.; Ma, Y., CALYPSO: A method for crystal structure prediction. *Comput. Phys. Commun.* **2012**, *183* (10), 2063-2070.

48. Gao, B.; Gao, P.; Lu, S.; Lv, J.; Wang, Y.; Ma, Y., Interface structure prediction via CALYPSO method. *Sci. Bull.* **2019**, *64* (5), 301-309.

49. Cheng, J.-G.; Matsubayashi, K.; Wu, W.; Sun, J.; Lin, F.; Luo, J.; Uwatoko, Y., Pressure induced superconductivity on the border of magnetic order in MnP . *Phys. Rev. Lett.* **2015**, *114* (11), 117001.

50. Hung, T. L.; Huang, C. H.; Deng, L. Z.; Ou, M. N.; Chen, Y. Y.; Wu, M. K.; Huyan, S. Y.; Chu, C. W.; Chen, P. J.; Lee, T. K., Pressure induced superconductivity in MnSe . *Nat. Commun.* **2021**, *12* (1), 5436.